The Most Sensitive SETI Observations Toward Barnard's Star with FAST

Zhen-Zhao Tao[1,2,3] , Bo-Lun Huang[1,2] , Xiao-Hang Luan[1,2] , Jian-Kang Li[1,2] , Hai-Chen Zhao[1,2] , Hong-Feng Wang[3], and
Tong-Jie Zhang (张同杰)[1,2,3]

[1] Institute for Frontiers in Astronomy and Astrophysics, Beijing Normal University, Beijing 102206, People's Republic of China; tjzhang@bnu.edu.cn
[2] Department of Astronomy, Beijing Normal University, Beijing 100875, People's Republic of China
[3] Institute for Astronomical Science, Dezhou University, Dezhou 253023, People's Republic of China

Abstract

Search for extraterrestrial intelligence (SETI) has been mainly focused on nearby stars and their planets in recent years. Barnard's star is the second closest star system to the Sun and the closest star in the Five-hundred-meter Aperture Spherical radio Telescope (FAST) observable sky which makes the minimum Equivalent Isotropic Radiated Power required for a hypothetical radio transmitter from Barnard's star to be detected by FAST telescope a mere 4.36×10^8 W. In this paper, we present the FAST telescope as the most sensitive instrument for radio SETI observations toward nearby star systems and conduct a series of observations to Barnard's star (GJ 699). By applying the multibeam coincidence matching strategy on the FAST telescope, we search for narrow-band signals (~Hz) in the frequency range of 1.05–1.45 GHz, and two orthogonal linear polarization directions are recorded. Despite finding no evidence of radio technosignatures in our series of observations, we have developed predictions regarding the hypothetical extraterrestrial intelligence signal originating from Barnard's star. These predictions are based on the star's physical properties and our observation strategy.

Unified Astronomy Thesaurus concepts: Astrobiology (74); Search for extraterrestrial intelligence (2127); Technosignatures (2128); Exoplanets (498)

1. Introduction

The Search for Extraterrestrial Intelligence (SETI) is a scientific endeavor aimed at detecting and studying potential signals from intelligent civilizations beyond Earth. The significance of SETI lies in its potential to answer one of the most profound questions in human history: are we alone in the universe? Since the pioneering work of Frank Drake and his eponymous equation in the early 1960s (Drake 1961), SETI has evolved into a diverse field encompassing radio and optical astronomy, astrobiology, and even the development of advanced technologies for interstellar communication (Shostak 2011). The discovery of thousands of exoplanets orbiting stars beyond our solar system has further invigorated the search for extraterrestrial life, as these distant worlds may harbor conditions suitable for the emergence of life as we know it (Seager 2013).

Narrowband radio SETI started as early as the 1960s (Drake 1961) because of several advantages. The natural and thermal broadening effect that makes signals produced by astrophysical sources possess a minimum width of hundreds of hertz (Cordes et al. 1997). Narrowband signals, on the other hand, are necessarily technologically modulated. As a result, narrowband signals can serve as technosignature of extraterrestrial intelligence (ETI) and can be distinguished from natural interference in the radio sky. Therefore, narrowband signals are the most searched type of signals in radio SETI (Siemion et al. 2013; Harp et al. 2016; Enriquez et al. 2017; Pinchuk et al. 2019; Price et al. 2020; Zhu et al. 2020; Gajjar et al. 2021; Traas et al. 2021; Tao et al. 2022).

The Five-hundred meter Aperture Spherical radio Telescope (FAST) is a groundbreaking instrument that has revolutionized our ability to explore the universe (Nan et al. 2011). Located in the Guizhou Province of China, FAST is the world's largest single-dish radio telescope. Its innovative design, which features an active reflector surface and a feed cabin suspension system, allows for unparalleled sensitivity and flexibility in observing a wide range of celestial phenomena (Jiang et al. 2019). Since its installation in 2016, FAST has played a crucial role in searching for radio signals from distant stars and galaxies (Zhang et al. 2020; Li et al. 2022; Tao et al. 2022; Luan et al. 2023). Its exceptional capabilities have enabled scientists to search for potential signs of ETI. Furthermore, the sensitivity of FAST is perfectly suitable for searching technosignatures from nearby stars. For an ETI transmitter inside Ross 128 system, the minimum Equivalent Isotropic Radiated Power (EIRP) that is required for FAST to detect is 1.48×10^9 W , which is even a few orders of magnitude less than the EIRP of the Arecibo Planetary Radar of $\sim 10^{13}$ W (Tao et al. 2022).

Barnard's Star is a red dwarf located in the constellation of Ophiuchus, approximately 1.8 pc away from our solar system (Gaia Collaboration et al. 2023). Named after the American astronomer Edward Emerson Barnard, who first observed its high proper motion in 1916 (Barnard 1916), this star has since become a subject of extensive study and speculation. As the second closest red dwarf to our solar system, after Proxima Centauri, Barnard's Star has garnered attention for its potential to host exoplanets and the possibility of harboring life (Anglada-Escudé et al. 2016). In recent years, the discovery of a candidate exoplanet, Barnard's Star b, has further fueled scientific curiosity and investigation. This super-Earth, with a minimum mass of 3.2 Earth masses, the maximum equilibrium temperature of the planet is 105 K , raising questions about its habitability and the potential existence of other planets in the
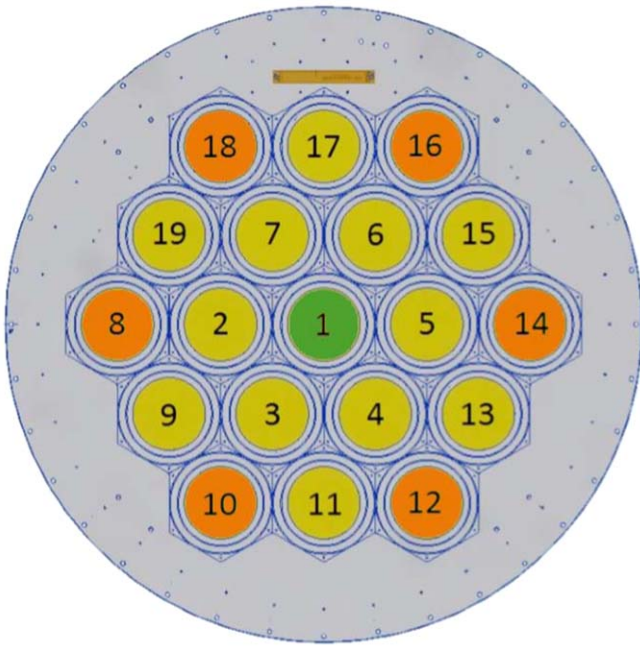
Figure 1. Schematic diagram of FAST's 19-beam receiver, the beam filled with green is Beam 1, which tracks the target star during the entire observation; the six outermost beams filled with orange are sufficiently separated from Beam 1 and act as the reference beams.

system (Ribas et al. 2018); however, Lubin et al. (2021) demonstrates that the planet candidate is most likely a false positive.

In this paper, we present the results of the SETI observations of Barnard's Star. In Section 2, we introduce the multi-beam coincidence matching (MBCM) strategy and the data collecting pipeline. The techniques we use to analyze our data are discussed in Section 3. The results are presented in Section 4. In Section 5, we discuss the sensitivity of our observations and a simple simulation of the ETI signal originating from Barnard's Star b. Finally, the conclusions of this work are presented in Section 6.

2. Observations

Identifying man-made radio frequency interference (RFI) has always been a major challenge in radio SETI, particularly in an era of increasing radio pollution. The ON-OFF strategy is employed in target observations to effectively identify RFI (Siemion et al. 2013; Enriquez et al. 2017; Pinchuk et al. 2019; Price et al. 2020; Sheikh et al. 2020; Gajjar et al. 2021; Smith et al. 2021; Traas et al. 2021), where intermittent observations of a reference position (OFF observation) are interleaved with observations of the target source (ON observation). The angular separation between the ON and OFF sources needs to be at least several times the telescope's half-power beamwidth to ensure that a sky-localized signal from the ON source is not detected during the OFF observations.

RFI signals are mostly not sky-localized, so they can be visible in both ON and OFF observations and thus can be directly eliminated. The MBCM strategy follows the same principle by taking the ON and OFF observation simultaneously with the FAST *L*-band 19-beam receiver (Tao et al. 2022; Luan et al. 2023). Only Beam 1 keeps tracking right on the target star, acting as the ON observation, whereas the six outermost beams (Beam 8, 10, 12, 14, 16, and 18) play the

roles of the OFF observations (Figure 1). We refer to the narrowband signals detected above a certain signal-to-noise ratio (S/N) threshold by any of the 19 beams as hits. Hits that possess an S/N greater than the threshold in the center beam but below the threshold in all the reference beams are called events. The signals detected by both Beam 1 and any of the reference beams are determined as RFI and rejected immediately. Using as many as six reference beams, we are able to remove the vast majority of signals detected by Beam 1.

On 2022 July 9th, 10th, 21st, and 28th, we conducted four individual observations of Barnard's Star with FAST, each with a duration of 20 minutes. We collected data in the frequency range of 1.0–1.5 GHz on the SETI back end, the number of frequency channels is 65536k, with a frequency resolution of approximately 7.5 Hz, and an integration time of 10 s for each spectrum. Each FITS file(Wells et al. 1981) contained data from four polarized channels (XX, YY, XY, YX) of two spectra per beam. The top and bottom 50 MHz are not within the designed frequency band of the receiver. Therefore, the effective data consists of a total bandwidth of 400 MHz, ranging from 1050 to 1450 MHz.

3. Data Analysis

There are currently two operating modes for the MBCM strategy: the standard targeted search mode which specifically focuses on a target star, and a blind search mode that extends the search area to the vicinity of the target star (Luan et al. 2023). Since this work is solely dedicated to Barnard's star, we choose the standard targeted mode rather than the blind search mode.

A narrowband signal transmitted from a distant source drifts in frequency due to the Doppler effect, and the drift rate is given by $\dot{\nu} = \nu_0 a/c$, where ν_0 is the original frequency of the signal, a is the relative acceleration between the transmitter and the receiver, and c is the speed of light. Thus Doppler drift represents a search parameter for narrowband SETI. Following Tao et al. (2022), we searched artificial narrowband signal data for two orthogonal linear polarization directions (XX and YY), using turboSETI (Enriquez et al. 2017; Enriquez & Price 2019). We convert the fits file obtained from observations into a filterbank file accessible by turboSETI. TurboSETI is a Python/Cython package using the tree search algorithm (Siemion et al. 2013) to search for narrowband signals. Two essential parameters required by turboSETI are an S/N threshold and a maximum drift rate (MDR), which allow turboSETI to search for narrowband signals above the S/N threshold within ±MDR.

It is essential to choose an appropriate value for the S/N threshold, setting an excessively high S/N can potentially filter out most of the received signals, which also increases the chance of filtering out an authentic ETI signal, whereas an insufficient S/N threshold can fail to filter out even some of the low S/N noises.

Since the drift rate of a signal is proportional to its original frequency, the suitable MDR depends on the observing frequency band, and 4 Hz s^{-1} is large enough for FAST *L*-band. Following Tao et al. (2022), we set the S/N threshold to 10 and the MDR to 4 Hz s^{-1}. TurboSETI outputs the best-fit frequencies, drift rates, and S/Ns of the hits detected by each beam to a DAT file.

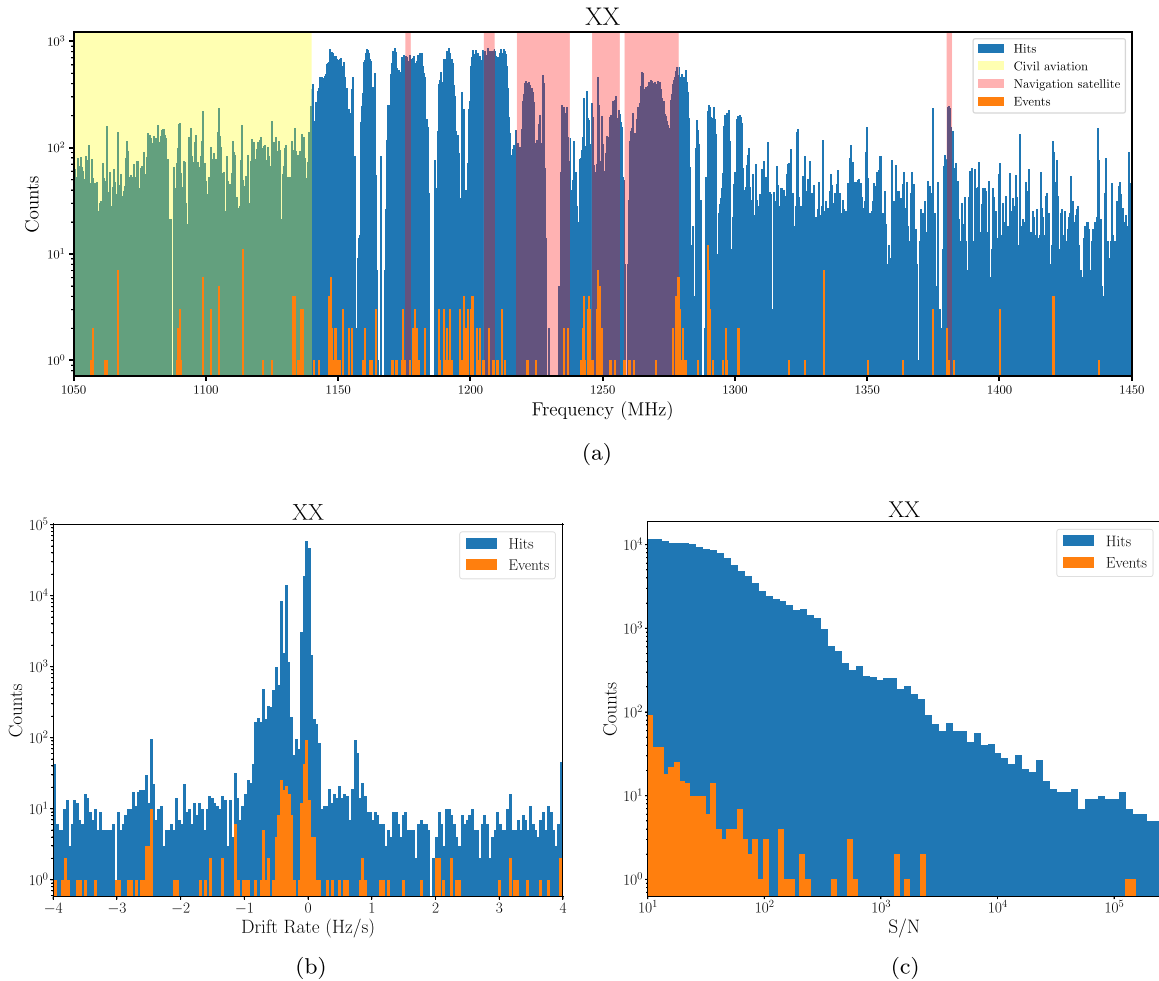We use the modified find_event_pipeline method of TurboSETI to search for hits that exist in beam 1, but not in

Figure 2. Histograms of hits and events for XX as functions of frequency, drift rate and S/N. Frequency bands of cataloged interference sources are displayed on the frequency panel. The blue bars show the distributions of the hits detected by all 19 beams. The orange bars show the distributions of the events detected by Beam 1.

the reference beams (Tao et al. 2022). TurboSETI outputs the selected events of each source to a CSV file. Since the effective bandwidth of the *L*-band receiver is 1.05–1.45 GHz (Nan et al. 2011), we discard events detected within the two unusable 50 MHz-wide ends of the band after event finding by turboSETI.

4. Results

We ran turboSETI on all observation data, finding 159,394 hits of XX polarization and 160,097 hits of YY polarization from all 19 beams. Of these, 367 events of XX and 317 events of YY were detected only in Beam 1. The distributions of frequency, drift rate, and S/N for the hits detected by all 19 beams and the events detected by Beam 1 are shown in Figures 2 and 3, and each figure displays one polarization direction. The general distribution trend of each parameter does not vary apparently with polarization direction, implying that most hits and events are not significantly polarized. According to the results of RFI environment tests at the FAST site, there are two major types of RFI sources within the 1.05–1.45 GHz frequency band, civil aviation and navigation satellites (Wang et al. 2021). We find only a small fraction of the hits falling within the civil aviation band (1030–1140 MHz). In contrast, hits within the navigation satellite bands (1176.45 ± 1.023 MHz, 1207.14 ± 2.046 MHz, 1227.6 ± 10 MHz,

1246.0–1256.5 MHz, 1268.52 ± 10.23 MHz, 1381.05 ± 1.023 MHz) account for a considerable proportion of the hits, implying that they are a major RFI source. Nondrift hits are in the majority as expected, since ground-based RFI sources are mostly stationary. The bias toward negative drift rate results from the downward relative acceleration vectors of non-geosynchronous satellites. The majority of the events have low S/N because weak RFI signals are likely to be detected below the S/N threshold by the reference beams but above the S/N threshold by Beam 1 accidentally, thus passing our event selection.

All the events selected by the program are re-examined by visual inspection of the dynamic timefrequency spectra (waterfall plots). we plot the dynamic spectra of the events using the BLIMPY package (Price et al. 2019), for beam 1 and reference beams. We reject events when it is clear by eye that the event was present in reference beams, but was not detected above the turboSETI $S/N > 10$ threshold. After visual inspection of these events, we found that all of them could be attributed to RFI. Most events are apparent false positives, they can be clearly seen in the reference beam. 21 events of XX and 28 events of YY, a total of 49 events were caused by instrument RFI (Tao et al. 2022). These frequencies can be linearly combined by the nominal frequencies (33.3333, 125.00 and 156.25 MHz) of the clock oscillators used by the Roach 2 FPGA board, so these events are attributed to the harmonics
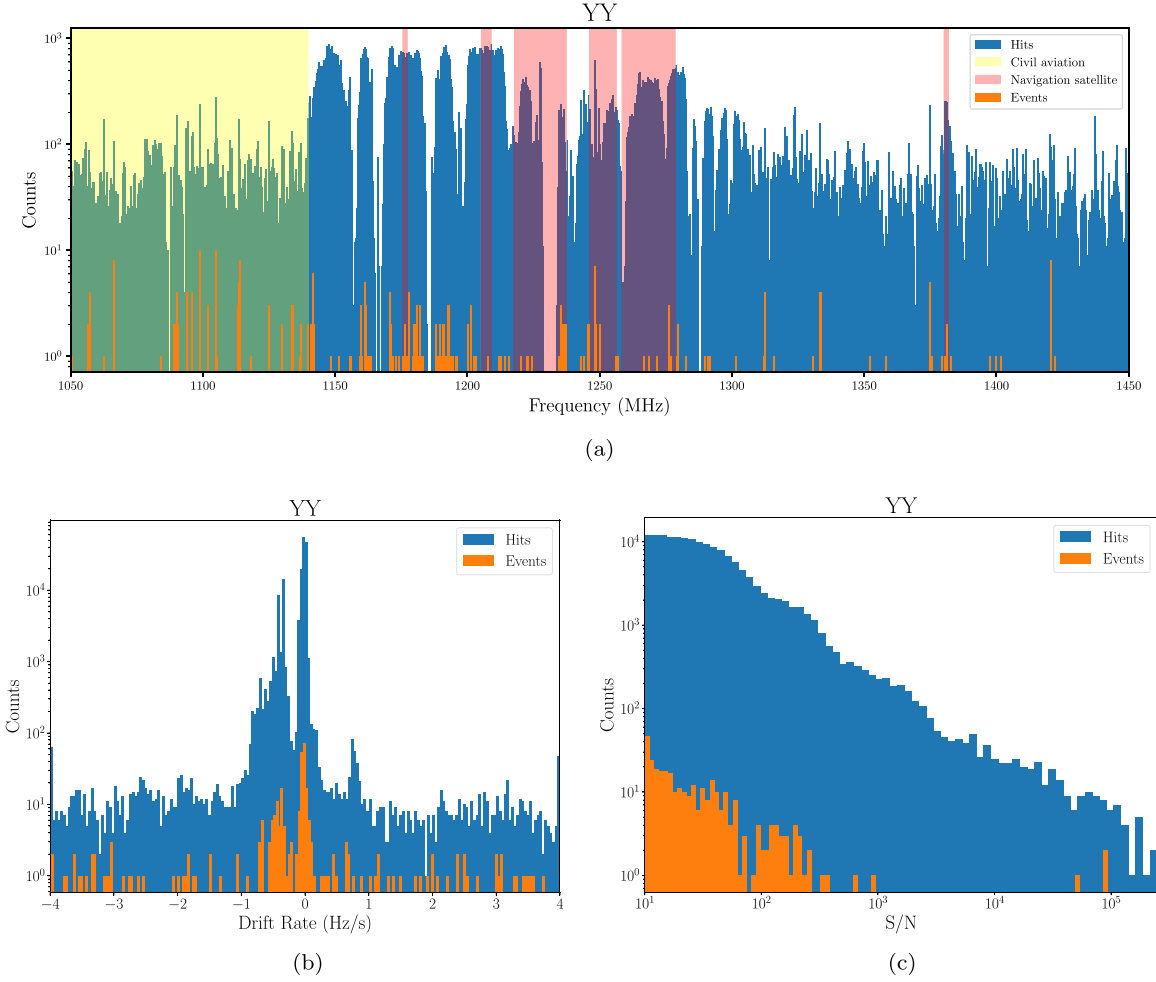
Figure 3. Histograms of hits and events for YY as functions of frequency, drift rate and S/N.

generated by the clock oscillators. So we attribute all the events to RFI.

5. Discussion

5.1. The Minimum Detectable EIRP from Barnard's Star

With the unprecedented sensitivity of FAST, we can thus compute the minimum detectable EIRP from Barnard's star, and it is defined as

$$\text{EIRP}_{\min} = 4\pi d^2 S_{\min}, \quad (1)$$

where d is the distance to the target. The Gaia Data Release 3 (Gaia Collaboration et al. 2023) shows the closest target in our observations, is 1.8 pc away. $S_{\min}$ is the minimum detectable flux. For extremely narrowband signal detection (where the bandwidth of the transmitter signal is narrower or equal to the spectral resolution of observation), the minimum detectable flux $S_{\min}$ is given by:

$$S_{\min} = \sigma_{\min} \frac{2k_{\mathrm{B}} T_{\mathrm{sys}}}{A_{\mathrm{eff}}} \sqrt{\frac{\delta\nu}{n_{\mathrm{pol}} t_{\mathrm{obs}}}}, \quad (2)$$

where $\sigma_{\min}$ is the S/N threshold, k_{B} is the Boltzmann constant, T_{sys} is the system temperature and A_{eff} is the effective collecting area. The ratio $A_{\mathrm{eff}}/T_{\mathrm{sys}}$ is also known as the sensitivity of the telescope. For the FAST L-band 19-beam

receiver, the sensitivity is reported to be $\sim$2000 m^2 K^{-1} (Nan et al. 2011; Li & Pan 2016; Jiang et al. 2019). $\delta\nu$ is the frequency resolution, n_{pol} is the polarization number, and t_{obs} is the observation duration (Enriquez et al. 2017). Due to the separate search of data for XX and YY, the polarization number is 1. It is worth noting that this expression is different from the $S_{\min}$ for observations aimed at astrophysical signals, where the signal bandwidth is wider than the frequency resolution, so the unit of $S_{\min}$ here is W m^{-2} rather than Jy (10^{-26} W m^{-2} Hz^{-1}). In this work, we observe the Barnard's star with a frequency resolution of $\sim$7.5 Hz and a observation time of 1200 s. The S/N threshold is set to 10.

We calculate $S_{\min} = 1.09 \times 10^{-26}$ W m^{-2} (1.09 Jy Hz) and $\text{EIRP}_{\min} = 4.36 \times 10^8$ W. For comparison, the EIRP of a typical Earth-based long-range radar transmitter is of the order of $\sim$10^9 W while a typical planetary radar is of the order of $\sim$10^{13} W. Barnard's Star b is a planet in the Barnard's Star system (Alvarado-Gómez et al. 2019). Assuming that there is a radio transmitter on Barnard's Star b and sends signals to us with EIRP of $\sim$10^9 W and $\sim$10^{13} W, we calculate the S/N of the signals observed by FAST to be in the order of $\sim$10 and $\sim$10^5 according to Function 1 and Function 2, respectively. We simulated such hypothetical ETI signal (Figure 4) using setigen (Brzycki et al. 2022).
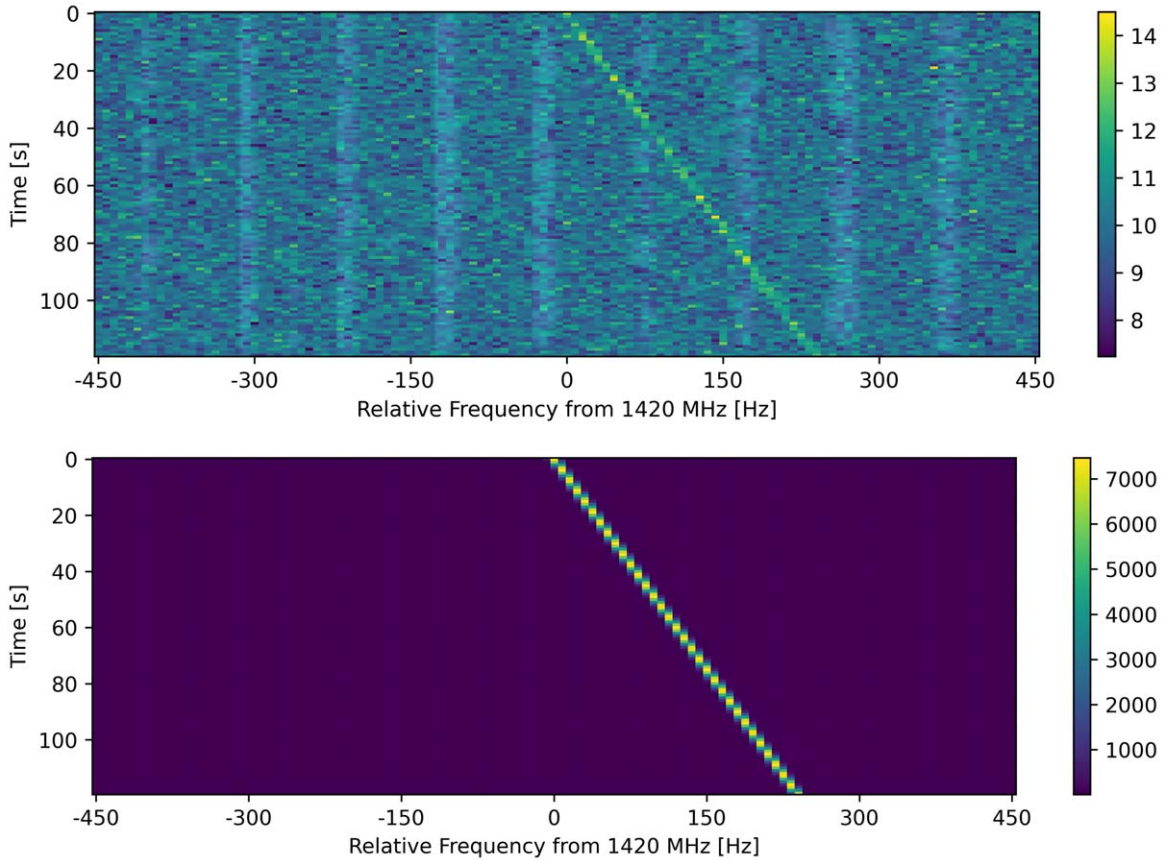
Figure 4. Simulated FAST received signals from radio transmitters of different powers on the surface of Barnard's Star B (drift rate is 0.2 Hz s^{-1}): top (EIRP $\approx 10^9$ W), bottom (EIR $\approx 10^{13}$ W).

5.2. Drift Rate Estimation of a Hypothetical Transmitter on Barnard's Star b

If the duty cycle of the radio transmitter on the surface of Barnard's star b is 100%, and the observation period can be long enough, the obtained ETI signal should fully or partially present a pseudosinusoidal curve. According to the parameters of Barnard's star b (Table 1) and Earth (Li et al. 2022), we simulated the long-term observation of Barnard's star, as shown in Figure 5, the asymmetry of the curve is caused by the high eccentricities of the exoplanets' orbits (Li et al. 2022). For the transmitter operating on the surface of Barnard's star b at 1420 MHz, the maximum drift rate we detected is 0.25 Hz s^{-1}.

FAST can easily detect weaker signals such as the communication signals we routinely generate from our long-range aircraft surveillance radars. Although factors such as whether extraterrestrial intelligence is sending a narrowband signal to Earth, and the duration of the transmission will make it impossible to predict the likelihood of detecting a signal. We can use the above frequency drift methods to verify a potential ETI signal of interest if we have enough observation time to carry out re-observation (Li et al. 2022).

6. Conclusions

FAST is the world's largest single-antenna radio telescope, SETI is one of its five science missions. Its extremely high sensitivity in the low-frequency radio L band is of great significance to SETI. Barnard's star is the second closest star system to the Sun and the closest star in FAST sky region

Table 1
Physical Properties of Barnard's Star b

Parameters	Value
Orbital period (d)	$232.80^{+0.38}_{-0.41}$
Eccentricity	$0.32^{+0.10}_{-0.15}$
Star mass($M_\odot$)	0.161 ± 0.0036
Orbital semimajor axis (au)	0.404 ± 0.018
R.A	$17^h57^m48\overset{s}{.}49847$
Decl.	$+04°41'36\overset{''}{.}1139$

Note. Orbital period, Eccentricity, and Orbital semimajor axis are from Ribas et al. (2018). Star mass is from Pineda et al. (2021). R.A and Decl. are from Gaia Collaboration et al. (2023). $M_\odot$ is the mass of the Sun. The rotation factor is ignored.

coverage. We conduct searches for narrowband drifting radio signals toward Barnard's star with FAST. Recording the data on the SETI back end with a frequency resolution of ~ 7.5 Hz, we search narrowband signals across 1.05–1.45 GHz with drift rates within ± 4 Hz s^{-1} and S/Ns above 10, in two orthogonal linear polarization directions separately. we calculate the minimum EIRP$_{min}$ = 4.36 × 10^8 W, which achieves an unprecedented sensitivity. This EIRP$_{min}$ is 7 times smaller than Green Bank Telescope observations of Barnard's star and 4.4 times smaller than Parkes Telescope observations of the closest star, Prox Cen (Smith et al. 2021). Although, our observations find no solid evidence for 100%-duty cycle radio transmitters emitting between 1.05 and 1.45 GHz with an EIRP above 4.36×10^8 W. Barnard's star remains an interesting target for
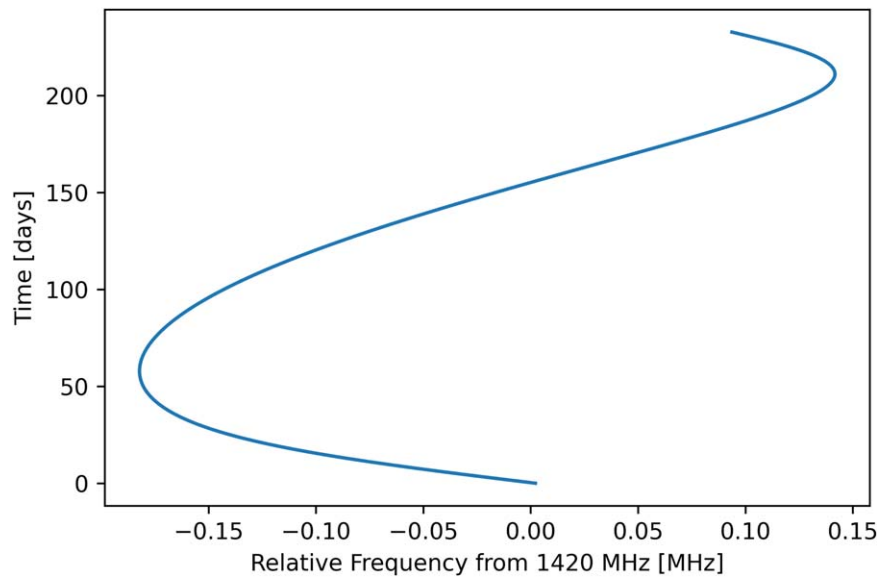
Figure 5. Pseudosinusoidal relative frequency curves of long-term observations for Barnard's Star b.

technosignature searches, and in the future, we will continue to observe it and search for more types of technical features such as periodic signals (Suresh et al. 2023). And we will conduct SETI surveys of more nearby stars as well as exoplanetary magnitude systems with FAST.

ORCID iDs

Zhen-Zhao Tao ⬤ https://orcid.org/0000-0002-4683-5500
Bo-Lun Huang ⬤ https://orcid.org/0000-0002-8719-3137
Xiao-Hang Luan ⬤ https://orcid.org/0000-0003-3977-4276
Jian-Kang Li ⬤ https://orcid.org/0000-0002-5485-1877
Hai-Chen Zhao ⬤ https://orcid.org/0000-0002-5485-1877
Tong-Jie Zhang
(张同杰) ⬤ https://orcid.org/0000-0002-3363-9965

References

Alvarado-Gómez, J. D., Garraffo, C., Drake, J. J., et al. 2019, ApJL, 875, L12
Anglada-Escudé, G., Amado, P. J., Barnes, J., et al. 2016, Natur, 536, 437
Barnard, E. E. 1916, AJ, 29, 181
Brzycki, B., Siemion, A. P. V., Pater, I. D., et al. 2022, AJ, 163, 222
Cordes, J. M., Lazio, J. W., & Sagan, C. 1997, ApJ, 487, 782
Drake, F. D. 1961, PhT, 14, 40
Enriquez, E., & Price, D. 2019, turboSETI: Python-based SETI Search Algorithm, Astrophysics Source Code Library, ascl:1906.006
Enriquez, J. E., Siemion, A., Foster, G., et al. 2017, ApJ, 849, 104
Gaia Collaboration, Vallenari, A., Brown, A. G. A., et al. 2023, A&A, 674, A1
Gajjar, V., Perez, K. I., Siemion, A. P. V., et al. 2021, AJ, 162, 33
Harp, G. R., Richards, J., Tarter, J. C., et al. 2016, AJ, 152, 181
Jiang, P., Yue, Y., Gan, H., et al. 2019, SCPMA, 62, 959502
Li, D., & Pan, Z. 2016, RaSc, 51, 1060
Li, J.-K., Zhao, H.-C., Tao, Z.-Z., Zhang, T.-J., & Xiao-Hui, S. 2022, ApJ, 938, 1
Luan, X.-H., Tao, Z.-Z., Zhao, H.-C., et al. 2023, AJ, 165, 132
Lubin, J., Robertson, P., Stefansson, G., et al. 2021, AJ, 162, 61
Nan, R., Li, D., Jin, C., et al. 2011, IJMPD, 20, 989
Pinchuk, P., Margot, J.-L., Greenberg, A. H., et al. 2019, AJ, 157, 122
Pineda, J. S., Youngblood, A., & France, K. 2021, ApJ, 918, 40
Price, D., Enriquez, J., Chen, Y., & Siebert, M. 2019, JOSS, 4, 1554
Price, D. C., Enriquez, J. E., Brzycki, B., et al. 2020, AJ, 159, 86
Ribas, I., Tuomi, M., Reiners, A., et al. 2018, Natur, 563, 365
Seager, S. 2013, Sci, 340, 577
Sheikh, S. Z., Siemion, A., Enriquez, J. E., et al. 2020, AJ, 160, 29
Shostak, S. 2011, AcAau, 68, 347
Siemion, A. P. V., Demorest, P., Korpela, E., et al. 2013, ApJ, 767, 94
Smith, S., Price, D. C., Sheikh, S. Z., et al. 2021, NatAs, 5, 1148
Suresh, A., Gajjar, V., Nagarajan, P., et al. 2023, AJ, 165, 255
Tao, Z.-Z., Zhao, H.-C., Zhang, T.-J., et al. 2022, AJ, 164, 160
Traas, R., Croft, S., Gajjar, V., et al. 2021, AJ, 161, 286
Wang, Y., Zhang, H.-Y., Hu, H., et al. 2021, RAA, 21, 018
Wells, D. C., Greisen, E. W., & Harten, R. H. 1981, A&AS, 44, 363
Zhang, Z.-S., Werthimer, D., Zhang, T.-J., et al. 2020, ApJ, 891, 174
Zhu, W., Li, D., Luo, R., et al. 2020, ApJL, 895, L6